© JUN 2026 | IRE Journals | Volume 9 Issue 12 | ISSN: 2456-8880
DOI: https://doi.org/10.64388/IREV9I12-1718796

Optimization of Hollow Shaft Geometry for Rotor Cooling in Inductions Motors Using Response Surface Methodology

ONYEJI LEVI CHINAKA[1], IBEZIM JOSEPH MADUABUCHI[2], DR SAMUEL O. IKEGBULA[3], UNYA NDUKWE[4]
[1]*Erisco Foods Limited*
[2,3]*Federal Polytechnic Nekede Owerri*
[4]*Standard Organization of Nigeria (SON)*

Abstract- ***Maintaining performance and dependability in induction motors requires efficient thermal management, especially as power density requirements rise in electric vehicle applications. Although direct rotor heat extraction is possible with hollow shaft cooling, systematic geometric optimisation that takes structural, hydraulic, and thermal trade-offs into account has not yet been investigated. This study optimizes hollow shaft geometry for a 120-kW induction motor using Response Surface Methodology (RSM) coupled with Computational Fluid Dynamics (CFD). Three variables were examined in relation to four responses: heat transfer coefficient, temperature reduction, pressure drop, and structural safety factor. These variables were fin density (15–25 fins/100 mm), channel aspect ratio (1.5–2.5), and coolant flow rate (4–8 L/min). A Central Composite Design with 20 experimental runs was employed. Coolant flow rate emerged as the dominant factor influencing all responses. Maximum thermal performance (709.6 W/m²·K, 18.07°C reduction) occurred at the highest factor levels but produced the lowest safety factor (1.753) and the highest pressure drop (22.98 kPa), confirming inherent design trade-offs. Linear models adequately predicted thermal responses, while pressure drop and safety factor exhibited significant curvature, requiring quadratic modeling. The optimized configuration balances thermal enhancement against hydraulic and structural constraints, providing a validated framework for hollow shaft cooling design in traction motors.***

Keywords: Induction Motor, Hollow Shaft Cooling, Response Surface Methodology, Thermal Management, Multi-Objective Optimization, Rotor Cooling

I. INTRODUCTION

The asynchronous motor is critical for modern industry, most notably the squirrel-cage induction motor, because of its ruggedness, high starting torque, and relatively low cost (Konda et al., 2024; Sethupathi & Senthilnathan, 2020). However, an ongoing challenge throughout the life of this machine has been managing and controlling the internal heat generated during operation (Q. Wang et al., 2022). There has been a growing desire for increased power density in many applications, especially as they pertain to electric vehicles; therefore, increased thermal management challenges are compounding this issue of heating within the motor assembly, thus creating excessive temperature, which ultimately limits the performance, reliability, and service life of the motor (Konovalov et al., 2023). More specifically, overheating at critical areas such as the rotor assembly causes accelerated degradation of the insulation film, increases electrical losses, and thus leads to premature motor failure. Based upon the Arrhenius rule, for every 10ºC that the operating temperature exceeds the motor's rated temperature, the lifespan of the insulation will be reduced to one-half (Rachman & Risdiyanto, 2015). Thus, effective cooling is not simply optional - it is a critical necessity for reliable operation (Onyegirim, 2025).

Natural convection, forced air, and housing-mounted water jackets are examples of traditional cooling techniques that have worked well for stator cooling but fall short for rotor assembly cooling (Gai, 2020). Since the rotor revolves, there isn't an easy way to transfer heat from the rotor to the motor casing, like there is from the stator, creating a thermal bottleneck at the rotor's air gap to the stator. This has led to new interest in developing ways to place cooling channels at the center of the motor and, thus, develop a more efficient internal cooling system. Hollow shaft technology is dramatically changing how we address this problem by allowing us to overcome the basic challenge by providing a direct path for heat to be removed from the core of a motor (Q. Wang et al., 2022). Using a hollow shaft, we can circulate a

coolant through a hollow shaft so that any heat generated from the rotor is directly transferred to the coolant and thus significantly decreases the thermal resistance compared to using a stator-jacket cooling system (Gundabattini & Mystkowski, 2022; R. Wang et al., 2022). Although hollow shaft cooling has a lot of potential, there is currently a huge gap in the literature around systematically optimizing the geometry of hollow shafts to create a direct relationship between their linear and geometric parameters and several performance measures. Most studies that have been conducted to date have utilized a parametric "one-factor-at-a-time" study, the results of which do not account for interaction effects and therefore do not produce true optimal configurations (Idogho et al., 2025; Nwigbo et al., 2025). Similarly, these studies have not quantified the various trade-offs between thermal (heat transfer coefficient, temperature reduction), hydraulic (pressure drop), and structural (safety factor) performance metrics.

Response Surface Methodology (RSM) is a very useful statistical tool to help overcome the above limitations (Ezechukwu et al., 2025; Jugu et al., 2025; Madukasi et al., 2025). RSM provides the ability to Design of Experiments (DOE) with multiple factors being varied at once (Okpala et al., 2025; Onyenanu & Nwigbo, 2021; Onyenanu et al., 2024a; Offodum et al., 2025; Onyenanu et al., 2024b), thereby allowing predictive modeling to be performed for main effects, interactions, and quadratic curvature, which will yield multi-objective optimization using desirability functions (Pereira et al., 2023; Petrova & Dimitrov, 2025; Shirazi et al., 2020). This study uses RSM and Computational Fluid Dynamics (CFD) to optimize three critical parameters (fin density, channel aspect ratio, and coolant flow rate) for a 120-kW induction motor with hollow-shaft cooling. The main objectives of this research study are to produce statistical models correlating these three parameters with the four conflicting responses (heat transfer coefficient, temperature reduction, pressure drop, and safety factor), determine the significance of each of the three independent factors, and identify the optimal setting for each of the independent factors that will maximize thermal performance while satisfying acceptable hydraulic and structural constraints.

II. LITERATURE REVIEW

In the literature review, previous studies of hollow shaft cooling options for asynchronous (induction) motors are reviewed. Emphasis will be placed on how the rotor maintains the heat and how conventional cooling systems have limitations, advanced internal cooling methods, as well as the computational and experimental methods used to analyze these systems (i.e., Computational Fluid Dynamics, Finite Element Analysis, and Conjugate Heat Transfer). The table below enumerates representative papers of those papers that highlight the lack of a systematic RSM-based multi-objective geometric optimization method(s) for induction motors, which the current study seeks to remedy via a comparative analysis of counter flow, fin-enhanced, and ducted designs.

Table 2.1: Summary of Key Studies on Hollow Shaft Cooling and Rotor Thermal Management in Induction Motors

Study Title	Key Focus	Methodology	Findings	Relevance to Study	Citations
Numerical prediction and measurement of pressure drop and heat transfer in a water-cooled hollow-shaft rotor for a traction motor application	Effects of rotation, flow rate, and temperature on thermal performance of hollow-shaft rotor cooling in traction motors	CFD modeling of rotational hollow shaft; HTC correlations for stationary vs. rotating cases	Rotation-induced heat transfer and pressure drop have been found to have two opposing impacts, either increasing or decreasing, based on CFD models and experimental prototype testing. The use of such a rotor cooling system is	Establishes rotational enhancement in hollow shafts; supports CFD for evaluating counter-flow and enhanced configurations in asynchronous motors	(Gai et al., 2021)

			found to result in a notable decrease in rotor temperature for an automobile traction motor.		
Thermal Analysis-Based Design of Hollow Shaft for Improved Cooling of Induction Motors	Design of hollow shaft for 75–120 kW induction motors to maintain component temperatures <100°C	Thermal modeling, CFD/FEA for counter-flow, fin-enhanced, and duct designs	Superior thermal performance and ease of manufacturing are provided by duct-based design, which also targets temperature limits and achieves notable HTC benefits. In addition, the heat transfer coefficient is 303% higher than in a counterflow arrangement.	Emphasises the effectiveness of direct rotor cooling and directly parallels thesis configurations and induction motor usage.	(Dinh, 2023)
Selecting Cooling Methods for Electric Motors	Quantitative comparison of cooling techniques using HTC and max heat flux as KPIs, including hollow shaft-based	Review and benchmarking of indirect/direct air, liquid jacket, hollow shaft, spray, etc.	Induction machine rotor cooling gaps are addressed by hollow shafts, which have a greater HTC than traditional jackets and emphasise the necessity for rotor-focused solutions.	Explains the differences between hollow shaft and conventional systems and argues for the need for enhanced internal cooling.	(Li et al., 2025)
A Review and Case of Study of Cooling Methods: Integrating Modeling, Simulation, and Thermal Analysis for a Model Based on a Commercial Electric Permanent Magnet Synchronous Motor	Review and case on shaft cooling in PMSM/IM; temperature reductions and efficiency gains	CFD/FEA simulation; hollow shaft configurations analysis	According to simulation studies, hybrid cooling considerably lowers the temperature of vital parts like permanent magnets and stator windings. Hollow shafts increase high-speed performance and lower rotor temperatures by 30–40°C and HTC 600–1200 W/m²·K.	The results demonstrate how well hybrid cooling systems work to maximise electric machine operational performance and thermal management. It facilitates the comparison of setups and the advantages of rotor temperature in asynchronous and induction settings.	(Usca-Gomez et al., 2025)
Model-based	Liquid shaft	CFD-based	Improved thermal	Relevant for RSM-	(Deriszadeh

design and optimization of a shaft cooling for an automotive electric motor	cooling model and parametric optimization under operational conditions	modeling; optimization of flow/geometry parameters	performance via shaft liquid cooling; insights into pressure drop vs. heat transfer trade-offs	like optimization of geometry/flow in shaft designs; bridges to multiobjective analysis	et al., 2024)
Power Losses and Thermal Analysis of a Hollow-Shaft Rotor Cooling System	Losses and thermal performance in hollow-shaft rotor cooling for traction motors	CFD/FEA coupled analysis; rotational effects on friction/heat transfer	Rotation enhances convection but increases losses; significant rotor cooling potential	Supports both empirical gaps in rotating hollow shafts and theoretical underpinnings (Nusselt correlations, Navier-Stokes).	(Gai et al., 2019)
Numerical and	Heat transfer	Numerical	Direct heat extraction	Complements the	(Lee, 2025)
Experimental	in a rotating	CFD +	from the rotor core and	thesis's CFD/FEA	
Analysis of	hollow shaft	experimental	verified HTC	approach and	
Heat Transfer in	for a traction	validation;	improvements with	validation needs for	
a Rotating	induction	focus on	rotation. In comparison	induction motor	
Hollow Rotor	motor	rotating	to the baseline unfinned	applications	
Shaft Cooling		channel	design, it is determined		
System for		convection	that the internally finned		
Electric Motor			design can deliver a lower		
Applications			shaft surface		
			temperature for lower		
			rotational speeds, with a		
			maximum temperature		
			decrease of 33.2°C in the		
			static condition.		

This table offers a side-by-side comparison of the results from eight different research papers that address the cooling of hollow-shaft rotors in electric motors by either computational fluid dynamics (CFD) simulations or physical experiments. The foundational principles concerning how rotational motion affects heat transfer and provides empirical verification of those principles from the Gai et al, (2021) and Gai et al, (2019) papers both show opposing effects on pressure losses due to volume flow rate as compared to a hollow shaft. The Dinh, (2023) paper provides empirical support of the thesis configurations, as the author found that the HTC of ducted cooling in induction motor configurations was greater than ducted cooling, with an increase of 303%. The Li et al (2025) paper provides a comparative review of HTC values for hollow shafts compared to jacketed cooling systems. The Usca-Gomez et al, (2025) paper found that by employing

hybrid cooling of PMSMs, there were approximately 30-40°C reductions in the attainable operating temperature of these motors and HTC increases ranging from 600 to 1200 W/m²·K. The Deriszadeh et al, (2024) paper presented parametric optimization for the first time, connecting the studies of flow and geometry to multi¬objective analysis. Finally, the Lee, (2025) paper provided empirical support for the trade-offs between increasing convection and resulting increase in rotational losses, thereby providing theoretical justification for the use of this cooling methodology.

III. METHODOLOGY

© JUN 2026 | IRE Journals | Volume 9 Issue 12 | ISSN: 2456-8880
DOI: https://doi.org/10.64388/IREV9I12-1718796

3.1 Research Design

The study uses a thorough experimental research strategy that combines design optimization techniques, computational fluid dynamics (CFD), and computer-aided design (CAD). Using a step-by-step exploratory methodology, the study begins with parametric modeling, proceeds to simulation analysis, and concludes with statistical optimization using Design Expert 13 to implement Response Surface Methodology (RSM).

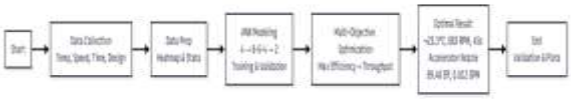

Figure 1: Flowchart of the RSM-Based Optimization Methodology for Hollow Shaft Geometry in Induction Motors

3.2 Materials and Properties

3.2.1 Material Selection and Properties

The hollow shaft is manufactured using AISI S5 shock-resistant tool steel (referred to also as SAE-AISI S5 or T41905). AISI S5 was chosen for its very good impact toughness, ductility, and suitability for rotor loads in induction motors used in electric vehicles (EVs). This type of tool steel will provide the necessary mechanical strength to the shaft without hindering its electromagnetic performance. Key properties of AISI S5 steel (quenched and tempered condition):

- Thermal conductivity: 42 W/m·K
- Specific heat capacity: 480 J/kg·K
- Density: 7,830 kg/m³
- Yield strength: up to 1,730 MPa (hardened)
- Hardness: 55–60 HRC

These properties ensure effective heat conduction from the rotor to the cooling channels while resisting deformation under high torque and rotational stresses. The cooling fluid is a 50%/50% Ethylene glycol-water mixture (by volume) due to the wider operational temperature range of this mixture (i.e., a freezing point of -37°C and boiling point of 107°C) compared to water. It will also act as an antifreeze and will maintain its thermal stability under automotive/EV operating conditions. Typical properties at 20°C are shown in Table 3.1.

Table 3.1: Comparative Properties of Key Materials

Property	AISI S5 Steel (Hardened)	50/50 EG-Water Mix (20°C)
Thermal Conductivity (W/m·K)	42	0.386
Specific Heat Capacity (J/kg·K)	480	3,410
Density (kg/m³)	7,830	1,070
Yield Strength (MPa)	1,730	N/A

These selections form the foundation for thermal and structural simulations, ensuring reliable heat extraction while maintaining mechanical stability.

3.3 Design Configurations, Constraints, and Parameters

3.3.1 Base Motor Specifications and Target Motors

The hollow shaft cooling system is designed for 75 kW and 120 kW induction motors (rear and front axle drives in an EV, total 195 kW). Initial modeling uses a 140-kW benchmark (e.g., Audi e-Tron motor) for framework validation, with adaptation planned once the EM team finalizes 75/120 kW loss profiles and dimensions.

Table 3.2: Dimensions and Rotor Losses (Example for 140 kW Baseline at Peak/Rated Speed)

Parameter	Value	Unit
Shaft diameter	70	mm
Stack length	210	mm
Inner cylinder diameter	22	mm
Rotor speed	924.9	rpm
Rotor losses (peak, rated speed)	2736.1	W

Table 3.3: Dimensions and Rotor Losses for Target 75 kW and 120 kW Motors (Selected Operating Points)

Parameter	75 kW Motor	120 kW Motor	Unit
Shaft diameter	65	70	mm

© JUN 2026 | IRE Journals | Volume 9 Issue 12 | ISSN: 2456-8880
DOI: https://doi.org/10.64388/IREV9I12-1718796

Stack length	204	248	mm
Rotor losses (continuous, rated speed)	674.3	612.6	W
Rotor losses (peak, rated speed)	2736.0	2404.3	W
Rotor losses (peak, max speed)	2023.5	4170.7	W

Thermal target: Maintain average component temperatures ≤ 100°C in steady-state.

3.3.2 Design Configurations and Variants

The predominant configuration of the hollow shaft is a counter-flow heat exchanger within a stationary internal cylinder (i.e., double pipe heat exchanger). Fluid will flow in the opposite direction in each of the pipes: one pipe (the internal cylinder) will be the fluid's primary travel path, whereas the other (the annulus) will be where the coolant travels. The shaft rotates with the rotor while the cylinder remains fixed in its position. In order to provide maximum conductivity between the cylinder and damper tube, the inner surface of the cylinder will be made of aluminium (k ≈ 200 W/m·k). Enhancements for the hollow shaft design include the implementation of longitudinal fins on the inner wall of the hollow cylinder to increase surface area and heat transfer. The design of these fins will be optimized to provide as much benefit from convection as possible while keeping the head loss due to flow through them to a minimum (this has been evaluated through the use of fin efficiency and CFD).

Table 3.4: Input Parameters for Preliminary Stationary Shaft Analysis (Example)

Parameter	Region	Nominal Value	Unit
Thermal conductivity	Inner cylinder	0.5791	W/m·K
Inlet temperature	Annulus gap	30	°C
Reynolds number	Inner cylinder	20,394	-
Flow rate	Both regions	10	LPM
Fluid	Both regions	Water	-

3.3.3 Boundary Conditions and Meshing

- Heat flux on outer shaft wall from rotor losses (air gap insulation directs heat inward).
- Insulated side walls; radial heat flow to fluid.
- No-slip condition at fluid-solid interfaces.
- Rotating domain (shaft at 3,000–14,000 rpm) modeled with moving mesh.
- Mesh is made up of free triangular boundary + boundary layers + swept elements along the length of the shaft. The optimal mesh (≈232,000 elements) produces less than 0.1% variation in heat transfer coefficient (HTC) from a finer mesh (quality ≈0.78).

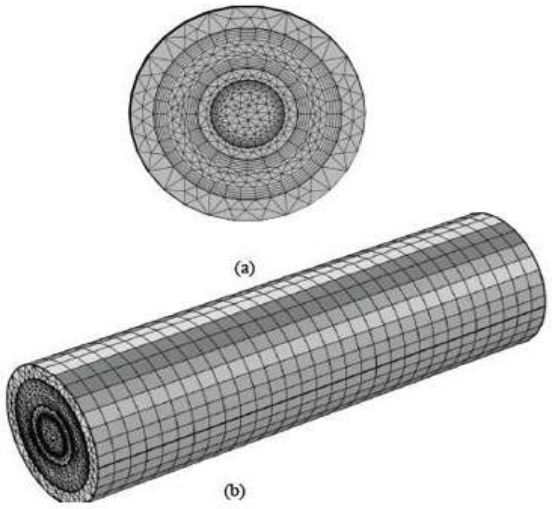

Figure 3.3: Meshing of hollow shaft (a) cross-sectional view (b) auxiliary view

3.4 Optimization Methodology

3.4.1 Response Surface Methodology (RSM)

The optimization of thermal and structural performance was performed using Response Surface Methodology (RSM), a statistical approach for modeling and analyzing the effects of multiple independent variables, including their interactions and curvature, on system responses. A Central Composite Design (CCD) was employed, ideal for three-factor experiments expecting quadratic effects.

Table 3.5. Factors and responses for CCD optimization

Variable	Factor	Range/Unit

© JUN 2026 | IRE Journals | Volume 9 Issue 12 | ISSN: 2456-8880
DOI: https://doi.org/10.64388/IREV9I12-1718796

Independent Variables		
X_1	Fin Density	15–25 fins/100 mm
X_2	Channel Aspect Ratio	1.5–2.5
X_3	Coolant Flow Rate	4–8 L/min
Dependent Variables		
Y_1	Heat Transfer Coefficient	W/m²·K
Y_2	Temperature Reduction	°C
Y_3	Pressure Drop	kPa
Y_4	Structural Safety Factor	-

This approach captures factor interactions and curvature effects while balancing thermal gains against hydraulic and structural constraints.

3.4.2 Design of Experiments (DOE)

A three-level factorial design with a total of 20 experimental runs was implemented to ensure a comprehensive exploration of the design space and statistically reliable results. The design consisted of 8 factorial points that represent the corner combinations of the independent variables, 6 axial points that extend beyond the factorial region to capture curvature effects, and 6 center points repeated at the midpoint of the design space to estimate pure error and improve model accuracy. The independent factors investigated were fin density (15–25 fins/100 mm), channel aspect ratio (1.5–2.5), and coolant flow rate (4–8 L/min), while the responses measured included heat transfer coefficient, temperature reduction in the rotor core, pressure drop, and structural safety factor. The experimental matrix was structured such that different combinations of these factors were systematically tested—for example, runs at lower fin density and coolant flow (Std 1, 9) contrasted with higher-density, higher-flow conditions (Std 6, 8, 19), and multiple center runs (Std15–20) were performed at X_1=20fins/100mm, X_2=2.0, and X_3=6L/min to improve the statistical robustness of the study. This arrangement not only captured the linear and interaction effects but also allowed quadratic terms to be modeled, thereby providing a strong foundation for response surface analysis and optimization.

Table 4.1: Incomplete Central Composite Design (CCD) of the Experiment

		Factor 1	Factor 2	Factor 3	Response 1	Response 2	Response 3	Response 4
Std	Run	A: Fin density	B: Channel aspect ratio	C: Coolant flow rate	Heat transfer coefficient	Temperature reduction in the rotor core	Pressure drops	Structural safety factor
		fins/100mm		L/min	W/m²·K	°C	kPa	
13	1	20	2	4				
10	2	25	2	6				
9	3	15	2	6				
15	4	20	2	6				
16	5	20	2	6				

© JUN 2026 | IRE Journals | Volume 9 Issue 12 | ISSN: 2456-8880
DOI: https://doi.org/10.64388/IREV9I12-1718796

20	6	20	2	6				
7	7	15	2.5	8				
6	8	25	1.5	8				
1	9	15	1.5	4				
11	10	20	1.5	6				
3	11	15	2.5	4				
12	12	20	2.5	6				
2	13	25	1.5	4				
17	14	20	2	6				
5	15	15	1.5	8				
19	16	20	2	6				
14	17	20	2	8				
4	18	25	2.5	4				
8	19	25	2.5	8				
18	20	20	2	6				

IV. RESULT

An experimental design of this investigation follows an organized structure where all run orders are randomized to reduce noise from external events, and in order for those results to come from factors that were controlled. Based on this design being a Central Composite Design (CCD), it is easy to see how it uses replicated center points (e.g., A=20, B=2, C=6) in order to allow for estimation of pure error as well as to conduct a Lack of Fit test to validate the model. It also has demonstrated (through the raw data) that the system has considerable complexity; there is a wide discrepancy between the Heat Transfer Coefficient (the coefficient is actually highest at maximum factor levels - 709.6 W/m2·K - and lowest at the minimum value of the Structural Safety Factor, which is 1.753).

Table 4.2: Central Composite Design (CCD) of the Experiment

		Factor 1	Factor 2	Factor 3	Response 1	Response 2	Response 3	Response 4

© JUN 2026 | IRE Journals | Volume 9 Issue 12 | ISSN: 2456-8880
DOI: https://doi.org/10.64388/IREV9I12-1718796

Std	Run	A: Fin density	B: Channel aspect ratio	C: Coolant flow rate	Heat transfer coefficient	Temperature reduction in the rotor core	Pressure drops	Structural safety factor
		fins/100mm		L/min)	W/m²·K	°C	kPa	
13	1	20	2	4	449.1	3.5	4.93	2.908
10	2	25	2	6	569.4	11.09	11.14	2.44
9	3	15	2	6	452.9	5.58	5.91	2.754
15	4	20	2	6	508	8.18	8.24	2.598
16	5	20	2	6	534.6	8.2	7.88	2.623
20	6	20	2	6	539.7	10.13	8.12	2.568
7	7	15	2.5	8	555.2	11.31	17	2.151
6	8	25	1.5	8	589.8	11.81	21.91	1.997
1	9	15	1.5	4	377.6	0.82	1.31	3.095
11	10	20	1.5	6	471.9	5.87	7.9	2.717
3	11	15	2.5	4	438.7	3.07	2.36	2.96
12	12	20	2.5	6	544.6	8.15	8.98	2.566
2	13	25	1.5	4	465.5	4.62	6.98	2.77
17	14	20	2	6	523.8	6.55	8.21	2.691
5	15	15	1.5	8	487.7	8.41	15.46	2.276
19	16	20	2	6	515.1	7.61	8.23	2.632
14	17	20	2	8	562.6	11.39	18.83	2.106
4	18	25	2.5	4	549.9	6.94	8.18	2.648
8	19	25	2.5	8	709.6	18.07	22.98	1.753
18	20	20	2	6	514.9	8.17	8.82	2.634

4.1 Heat Transfer Coefficient

4.1.1 ANOVA For Linear Model

The ANOVA results indicate that the linear model is statistically significant ($p < 0.0001$, F-value 148.43). All three factors tested (fin density, channel aspect ratio, and coolant flow rate) are statistically significant ($p < 0.05$), meaning that they all reliably influence heat transfer. The non-significant lack of fit

© JUN 2026 | IRE Journals | Volume 9 Issue 12 | ISSN: 2456-8880
DOI: https://doi.org/10.64388/IREV9I12-1718796

($p = 0.3668$) demonstrates that there is no evidence of curvature or un-modeled complexity, indicating that the linear model provides a good fit for the data and can be used for predictions within the experimental ranges.

Table 4.3: ANOVA for Response 1: Heat transfer coefficient

Source	Sum of Squares	df	Mean Square	F-value	p-value	
Model	88122.95	3	29374.32	148.43	< 0.0001	significant
A-Fin density	32729.84	1	32729.84	165.38	< 0.0001	
B-Channel aspect ratio	16443.02	1	16443.02	83.09	< 0.0001	
C-Coolant flow rate	38950.08	1	38950.08	196.81	< 0.0001	
Residual	3166.50	16	197.91			
Lack of Fit	2399.99	11	218.18	1.42	0.3668	not significant
Pure Error	766.51	5	153.30			
Cor Total	91289.44	19				

Factor coding is coded.
Sum of squares is Type III – Partial.

The Model F-value of 148.43 indicates significance, with only a 0.01% chance that this large value could occur from noise. Factors A, B, and C are all significant ($p < 0.05$). The non-significant Lack of Fit ($F=1.42$, $p=0.3668$) is desirable, with a 36.68% chance this F-value could occur from noise, confirming the model fits well.

4.1.2 Predicted and Actual Graph

Figure 2 is a critical diagnostic tool, plotting the model's predicted values against the actual measured values from the experiments. The data points clustering closely around the diagonal line indicate a strong agreement between the model and reality, confirming the model's predictive accuracy. Run 19, for example, is flagged for strong influence, suggesting it should be reviewed, but its impact is not severe enough to invalidate the overall strong model.

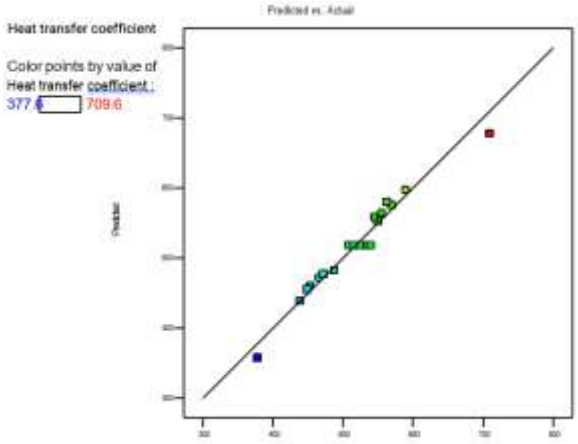

Figure 2: Illustrates the Correlation Between Predicted and Actual Values

4.1.3 Effect of Reinforcement Variables on Heat Transfer Coefficient.

The set of images (A, B, C, D) visually depicts the main effects of each factor on the Heat Transfer Coefficient. These plots would typically show a line where the slope indicates the strength and direction of the effect. A steep upward slope for Coolant Flow Rate (C) would confirm its dominant positive effect, meaning that increasing the flow rate consistently and

© JUN 2026 | IRE Journals | Volume 9 Issue 12 | ISSN: 2456-8880
DOI: https://doi.org/10.64388/IREV9I12-1718796

significantly improves heat transfer. Similarly, positive slopes for Fin Density (A) and Channel Aspect Ratio (B) would show that increasing these also enhances performance, albeit to a lesser degree than flow rate. These graphs provide an immediate, intuitive understanding of the factor effects, complementing the numerical ANOVA results

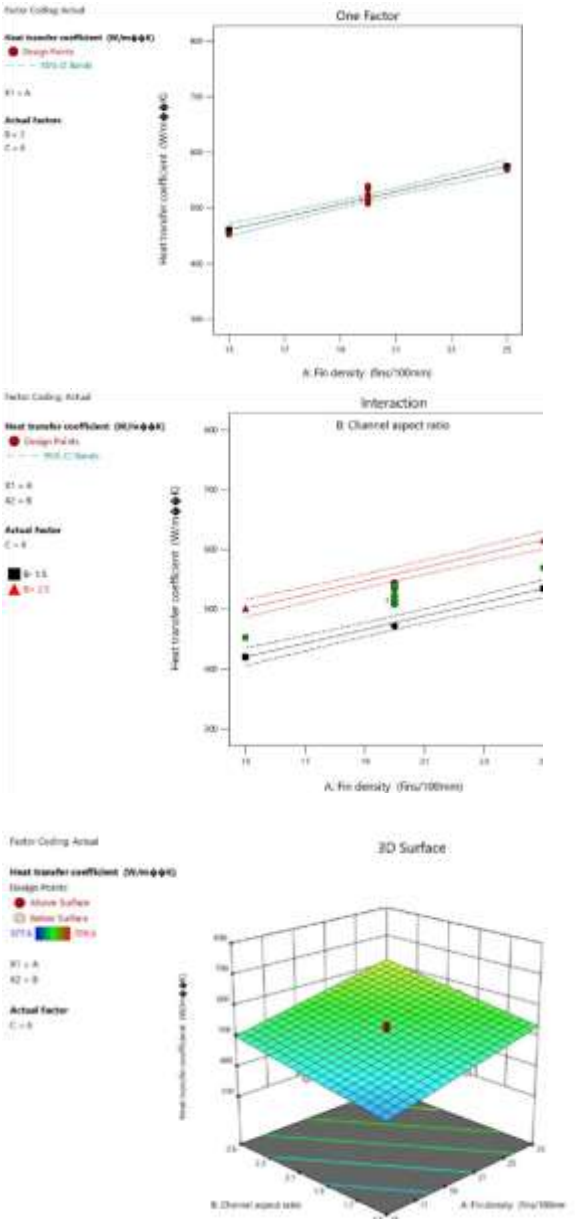

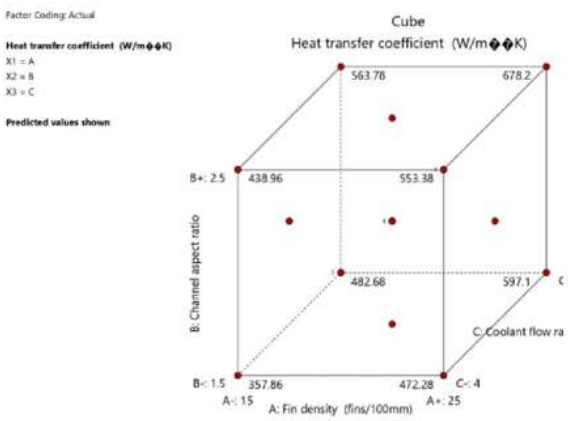

Figure 3: The main effects of each factor on the Heat Transfer Coefficient.

4.3 Temperature Reduction in Rotor Core

The empirical modeling and optimization of a rotor cooling system. It moves beyond theoretical assumptions to establish quantitative, data-driven relationships between key design parameters and system performance metrics. The analysis employs Response Surface Methodology (RSM), a powerful statistical technique, to dissect how Fin Density (A), Channel Aspect Ratio (B), and Coolant Flow Rate (C) individually and collectively influence Thermal Performance (Heat Transfer Coefficient and Temperature Reduction), Hydraulic Cost (Pressure Drop), and Structural Integrity (Safety Factor).

4.2.1 ANOVA For 2FI Model

The two-factor interaction (2FI) model in the ANOVA analysis for each temperature reduction was found to be highly significant (F-value = 46.06; $p < 0.0001$). The Sum of Squares, which quantifies the contributions from each of the factors, shows that the Coolant Flow Rate (C) alone represents 176.74 units, whereas Fin Density (A) and Channel Aspect Ratio (B) contributed only 54.48 and 25.63 units, respectively. This establishes that the Flow Rate is the most effective degree of freedom for producing heat. Additionally, all of the factor combinations AB, AC, and BC produced non-significant results ($p > 0.10$), suggesting that these interactions are additive rather than synergistic. The non-significant Lack of Fit statistic ($p = 0.8100$) indicates that the model fits the data appropriately without any unaccounted curvature.

© JUN 2026 | IRE Journals | Volume 9 Issue 12 | ISSN: 2456-8880
DOI: https://doi.org/10.64388/IREV9I12-1718796

Table 4.4: ANOVA for Response 2: Temperature reduction in rotor core

Source	Sum of Squares	df	Mean Square	F-value	p-value	
Model	261.72	6	43.62	46.06	< 0.0001	significant
A-Fin density	54.48	1	54.48	57.52	< 0.0001	
B-Channel aspect ratio	25.63	1	25.63	27.06	0.0002	
C-Coolant flow rate	176.74	1	176.74	186.61	< 0.0001	
AB	1.47	1	1.47	1.55	0.2347	
AC	0.7750	1	0.7750	0.8183	0.3821	
BC	2.63	1	2.63	2.78	0.1193	
Residual	12.31	13	0.9471			
Lack of Fit	5.54	8	0.6921	0.5108	0.8100	not significant
Pure Error	6.78	5	1.36			
Cor Total	274.04	19				

Factor coding is coded.
Sum of squares is Type III – Partial.

The Model F-value of 46.06 indicates significance, with only a 0.01% chance that this large value could occur from noise. Factors A, B, and C are all significant ($p < 0.05$). The non-significant Lack of Fit ($F=0.51$, $p=0.8100$) indicates the model fits well, with an 81% chance this F-value could occur from noise.

4.2.2 Predicted and actual Graph

Figure 5, the Predicted vs. Actual graph, would visually demonstrate a strong correlation, with data points clustered closely around a diagonal line, confirming the model's predictive accuracy. The image also identifies points with high leverage (noted with (1)), such as Runs 7, 8, and 9. A high-leverage point is one whose factor settings are at the extreme boundaries of the experimental design (e.g., all factors at low or high levels). These points have greater potential to "pull" the regression model toward them. While not necessarily bad, they are influential. This is further quantified by the DFFITS values; for example, Run 11 has a DFFITS of 2.410, which exceeds typical thresholds, suggesting it has a strong influence on the predicted values. These diagnostics are crucial for understanding the model's limitations and identifying any potentially anomalous data.

Predicted vs. Actual

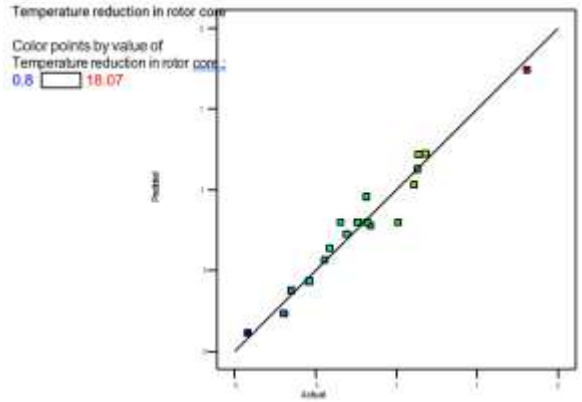

Figure 5: Illustrates the Correlation Between Predicted and Actual Values

© JUN 2026 | IRE Journals | Volume 9 Issue 12 | ISSN: 2456-8880
DOI: https://doi.org/10.64388/IREV9I12-1718796

4.2.3 Effect of Reinforcement Variables on Temperature Reduction

The four images in Figure 6 would typically include a main effects plot and interaction plots. The main effects plot would show three lines, one for each factor. The line for Coolant Flow Rate (C) would have the steepest positive slope, graphically confirming that increasing flow rate causes the largest increase in temperature reduction. The line for Fin Density (A) would also show a positive slope, but less steep, and similarly for Channel Aspect Ratio (B). The interaction plots would likely show near-parallel lines, which visually represent the lack of significant interaction—the effect of one factor remains consistent across different levels of another factor.

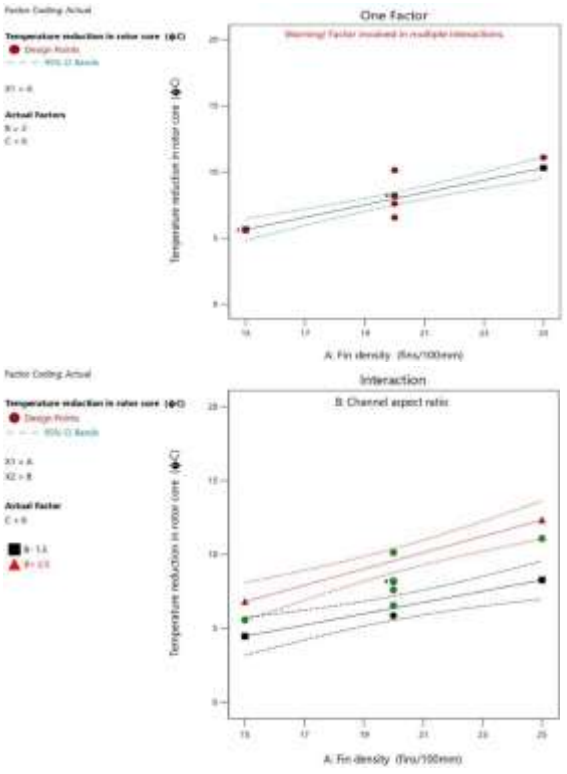

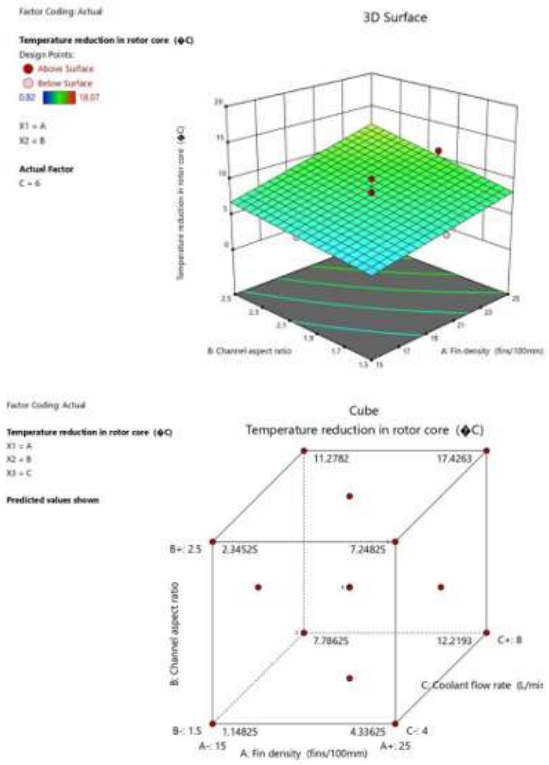

Figure 6: The main effects of each factor on the Temperature Reduction

4.3 Pressure Drop

Pressure drop analysis evaluates hydraulic losses in cooling channels, crucial for pump sizing and efficiency in motors. Values range 1.31-22.98 kPa, increasing with factors. Linear model suits, but a significant lack of fit suggests unmodeled curvature, common in rotating systems

4.3.1 ANOVA For Linear Model

In the ANOVA (Table 4.5) for Pressure Drop, the Significant Linear Model ($F=48.12$; $p<0.0001$) has Significant Fin Density (A) and Coolant Flow Rate (C); while the Aspect Ratio (B) is not Significant ($p=0.3755$). However, there is a Significant Lack of Fit ($p=0.0001$), which indicates that the Linear Model does not fit the true relationship, and it is likely Curvilinear with the Pressure Drop Increasing Non-Linear with the Flow Rate, so the Quadratic Model is the best for making predictions.

Table 4.5: ANOVA for Response 3: Pressure drop

© JUN 2026 | IRE Journals | Volume 9 Issue 12 | ISSN: 2456-8880
DOI: https://doi.org/10.64388/IREV9I12-1718796

Source	Sum of Squares	df	Mean Square	F-value	p-value	
Model	612.97	3	204.32	48.12	< 0.0001	significant
A-Fin density	84.97	1	84.97	20.01	0.0004	
aspect ratio	3.53	1	3.53	0.8310	0.3755	
	524.47	1	524.47	123.53	< 0.0001	
Residual	67.93	16	4.25			
	67.45	11	6.13	63.77	0.0001	significant
Pure	0.4808	5	0.0962			
Cor Total	680.90	19				

Factor coding is coded.
Sum of squares is Type – III Partial.

The Model F-value of 48.12 confirms significance, with only a 0.01% probability this magnitude arises from noise. Factors A and C are significant ($p < 0.05$). The Lack of Fit F-value of 63.77 is highly significant ($p < 0.0001$), indicating the linear model inadequately captures the true response surface.

4.3.2 Predicted and Actual Graph

The Predicted vs. Actual graph (Figure 7) would likely show a more scattered distribution of points around the diagonal line compared to the temperature reduction plot, a visual manifestation of the significant lack of fit.

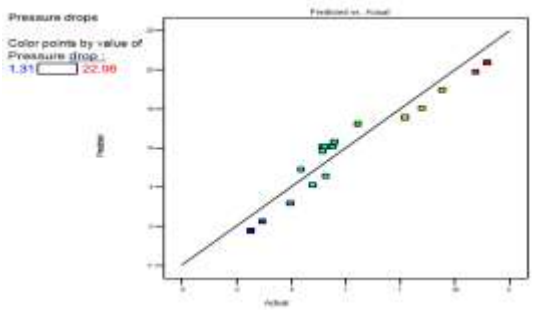

Figure 7: Illustrates the Correlation Between Predicted and Actual Values

4.3.3 Effect of Reinforcement Variables on Pressure Drop

Figure 8's primary impact charts show how each component affects the pressure decrease. Since pressure drop increases with the square of flow velocity, coolant flow rate (C) exhibits the steepest positive slope and is the primary hydraulic driver. The fin density (A) has a moderately positive slope; while more fins improve heat transmission, they also increase flow resistance due to friction and blockage. Its statistical insignificance ($p=0.3755$) and negligible effect on pressure loss are confirmed by the Channel Aspect Ratio's (B) almost flat appearance. Important hydraulic trade-offs are shown in these plots: increasing flow rates or using denser fins to achieve heat advantages results in pressure drop penalties, whereas changing the aspect ratio has negligible costs and benefits.

© JUN 2026 | IRE Journals | Volume 9 Issue 12 | ISSN: 2456-8880
DOI: https://doi.org/10.64388/IREV9I12-1718796

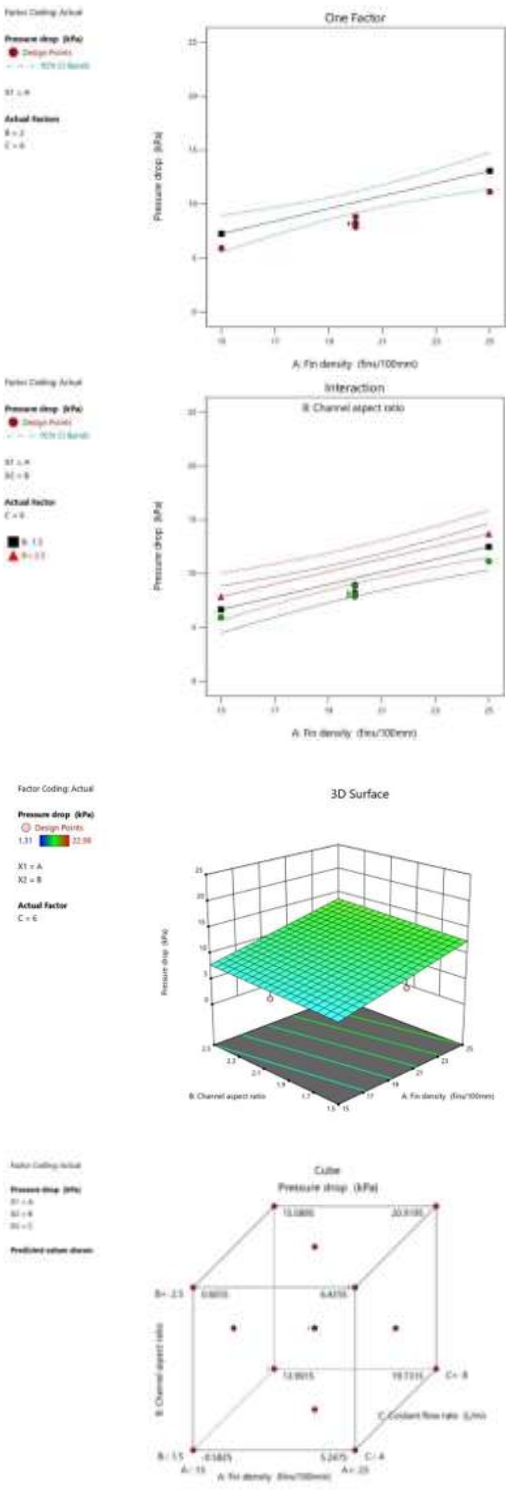

Figure 8: The main effects of each factor on the Pressure Drop

4.4 Structural Safety Factor

ANOVA for Structural Safety Factor shows a significant linear model ($F=75.41$, $p<0.0001$) with all factors statistically significant. All coefficients are negative, revealing a critical trade-off: thermal improvements compromise structural integrity. Coolant Flow Rate (C) has the strongest negative influence (Sum of Squares=1.68), likely from increased pressure loads or thermal stresses. Fin Density (A) also negatively impacts safety, probably through material removal, creating stress concentrations.

4.4.1 ANOVA For Linear Model

The ANOVA (Analysis of Variance) results on the Structural Safety Factor show that there is a statistically significant linear model with an F-value of 75.41 and a p-value of less than 0.0001. The coefficients for all factors are statistically significant but have negative values. This indicates that there is a trade-off between thermal enhancements and structural integrity. The Coolant Flow Rate (C) has the largest negative effect on the safety of the system, due to the increased pressures or thermal stresses associated with cooling the part. The Fin Density (A) also hurts the safety of the system and is likely due to the removal of material, causing stress concentrations. There is a significant Lack of Fit ($p=0.0208$), which indicates that the linear model is too simplistic for this complex structural response and there may be curvature or interactions that are not captured in the linear model.

Table 4.6: ANOVA for Response 4: Structural safety factor

Source	Sum of Squares	df	Mean Square	F-value	p-value	
Model	2.00	3	0.6683	75.41	< 0.0001	significant

© JUN 2026 | IRE Journals | Volume 9 Issue 12 | ISSN: 2456-8880
DOI: https://doi.org/10.64388/IREV9I12-1718796

A-Fin density	0.2650	1	0.2650	29.91	< 0.0001	
B-Channel aspect ratio	0.0604	1	0.0604	6.81	0.0189	
C-Coolant flow rate	1.68	1	1.68	189.50	< 0.0001	
Residual	0.1418	16	0.0089			
Lack of Fit	0.1333	11	0.0121	7.16	0.0208	significant
Pure Error	0.0085	5	0.0017			
Cor Total	2.15	19				

Factor coding is coded.
Sum of squares is Type – III Partial.

The Model F-value of 75.41 indicates significance, with only a 0.01% chance that this large value could occur from noise. Terms A, B, and C are significant ($p < 0.05$). The Lack of Fit F-value of 7.16 is significant (p=0.0208), with only a 2.08% chance this could occur from noise.

4.4.2 Predicted and Actual Graph

The predicted vs. actual graph (Figure 8) would show a reasonable correlation, but the significant lack of fit might manifest as a slight non-random pattern in the residuals. This diagnostically highlights the most critical boundary of the design space: the configuration for best cooling corresponds to the worst-case scenario for structural integrity.

This must be a primary consideration in any optimization effort.

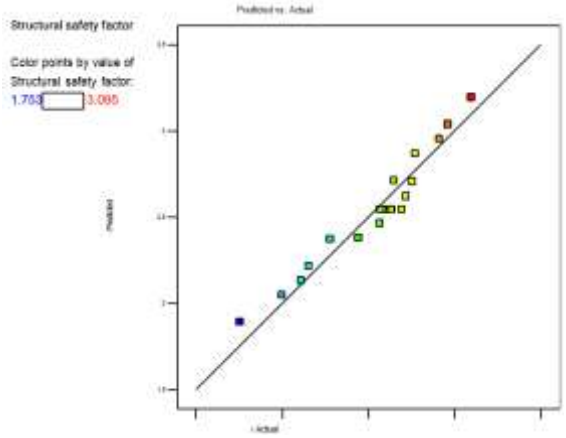

Figure 8: Illustrates the Correlation Between Predicted and Actual Values

4.4.3 Effect of Reinforcement Variables on Structural Safety Factor

The main effects plots in Figure 9 would graphically tell the story of compromise. All three plots would show downward-sloping lines. The line for Coolant Flow Rate (C) would have the steepest negative slope, visually reinforcing that it is the most detrimental factor to structural safety. The lines for Fin Density (A) and Channel Aspect Ratio (B) would also slope downwards, confirming that any design change aimed at improving thermal performance comes at the direct expense of reducing the safety margin against structural failure. These plots provide an immediate, intuitive understanding of the tough choices facing the designer.

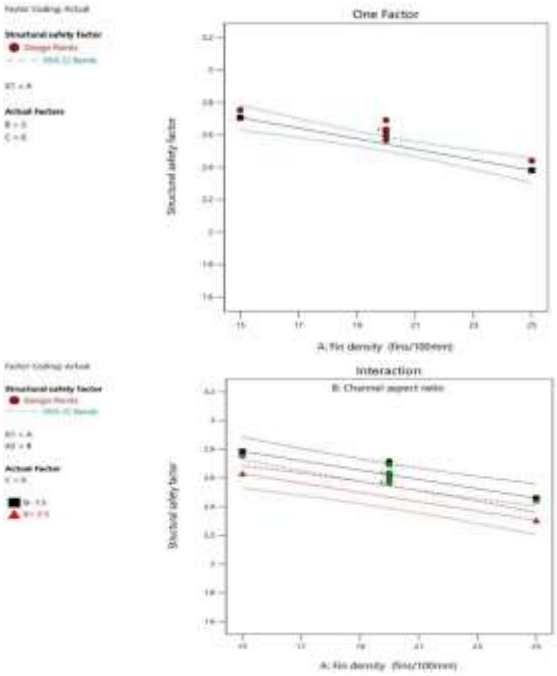

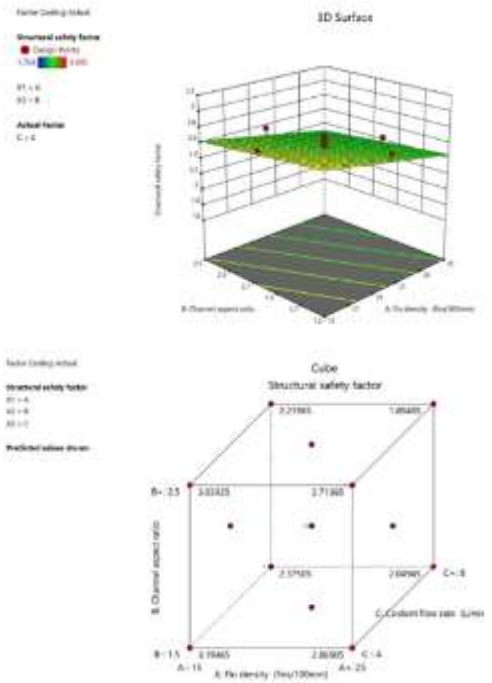

Figure 9: The main effects of each factor on the Structural Safety Factor

V. CONCLUSION

This study successfully employed Response Surface Methodology to optimize hollow shaft geometry for induction motor rotor cooling. Statistical analysis revealed that coolant flow rate is the dominant factor influencing all performance metrics, with the highest heat transfer coefficient (709.6 W/m²·K) and maximum temperature reduction (18.07°C) achieved at maximum factor levels (25 fins/100 mm, aspect ratio 2.5, 8 L/min). However, this optimal thermal configuration concurrently yielded the lowest structural safety factor (1.753) and highest pressure drop (22.98 kPa), confirming the fundamental trade-off inherent in rotor cooling design. All three factors significantly affect heat transfer and temperature reduction, while channel aspect ratio proved insignificant for pressure drop. The significant lack of fit in pressure drop and structural safety factor models indicates curvature requiring quadratic modeling. The linear models for heat transfer coefficient and temperature reduction demonstrated excellent predictive capability with a non-significant lack of fit, validating their utility for design space exploration. Based on these findings, future work should implement:

- Implement quadratic modeling for pressure drop and structural safety factor responses to capture curvature effects and improve prediction accuracy.
- Conduct multi-objective optimization using desirability functions to identify Pareto-optimal configurations balancing thermal performance against hydraulic and structural constraints.
- Validate optimized configurations experimentally through prototype testing under actual operating conditions.

REFERENCES

[1] Believe O Idogho, Ifeanyichukwu U Onyenanu, Kennedy C Owuama, Ashimedua C Ndubisi, Chukwunwendu E Ilochonwu (2025) Optimization of a Sustainable Virgin Coconut Oil Extraction Machine for Rural Communities. JournalofFood Technology&NutritionSciences. SRC/JFTNS-275. DOI: doi.org/10.47363/JFTNS/2025(7)215

[2] Deriszadeh, A., Di Battista, D., Di Giovine, G., & Cipollone, R. (2024). Model based design and optimization of a shaft cooling for automotive electric motor. Journal of Physics: Conference Series, 2893(1), 012124. https://doi.org/10.1088/1742-6596/2893/1/012124

[3] Dinh, I. (2023). Thermal Analysis Based Design of Hollow Shaft for Improved Cooling of Induction Motors. https://uwindsor.scholaris.ca/items/0d9285a0-ef1d-4ad4-8a74-22ae8f6c629a

[4] Ezechukwu, V. C., Oghenekaro, P. O., Onyenanu, I. U., Ayadinuno, G., & Agwaziam, J. O. (2025). Mathematical Modeling and Optimization of Plantain Chip Drying: A Parametric Study on Air Frying Conditions. IPS Journal of Engineering and Technology, 1(1). https://doi.org/10.54117/ijet.v1i1.13

[5] Gai, Y. (2020). A hollow-shaft rotor cooling system for automotive traction motors [PhD

Thesis, Newcastle University]. http://theses.ncl.ac.uk/jspui/handle/10443/5024

[6] Gai, Y., Chong, Y. C., Adam, H., Goss, J., & Popescu, M. (2019). Power losses and thermal analysis of a hollow-shaft rotor cooling system. 2019 22nd International Conference on Electrical Machines and Systems (ICEMS), 1–6. https://doi.org/doi:%252010.1109/ICEMS.2019.8922026.

[7] Gai, Y., Ma, C., Xu, Y., & Chong, Y. C. (2021). Numerical prediction and measurement of pressure drop and heat transfer in a water-cooled hollow-shaft rotor for a traction motor application. IET Electric Power Applications, 15(4), 476–486. https://doi.org/10.1049/elp2.12042

[8] Gundabattini, E., & Mystkowski, A. (2022). Review of air-cooling strategies, combinations and thermal analysis (experimental and analytical) of a permanent magnet synchronous motor. Proceedings of the Institution of Mechanical Engineers, Part C: Journal of Mechanical Engineering Science, 236(1), 655–668. https://doi.org/10.1177/0954406220987267

[9] Jugu, E. B., Onyenanu, I. U., & Nwobi-Okoye, C. C. (2025). Finite Element Analysis and Factorial Optimization of Heat Treatment Flaws in CNG Pressure Vessels: Implications for Structural Integrity and Safety. ScientificJournalofEngineering, andTechnology, 2(1). https://doi.org/10.69739/sjet.v2i1.487

[10] Konda, Y. R., Ponnaganti, V. K., Reddy, P. V. S., Singh, R. R., Mercorelli, P., Gundabattini, E., & Solomon, D. G. (2024). Thermal Analysis and Cooling Strategies of High-Efficiency Three-Phase Squirrel-Cage Induction Motors—A Review. Computation, 12(1), 6. https://doi.org/10.3390/computation12010006

[11] Konovalov, D., Tolstorebrov, I., Eikevik, T. M., Kobalava, H., Radchenko, M., Hafner, A., & Radchenko, A. (2023). Recent Developments in Cooling Systems and Cooling Management for Electric Motors. Energies, 16(19), 7006. https://doi.org/10.3390/en16197006

[12] Lee, M. (2025). Numerical and Experimental Analysis of Heat Transfer in a Rotating Hollow Rotor Shaft Cooling System for Electric Motor Applications. https://uwindsor.scholaris.ca/items/5f8b6803-e9b4-4ea5-96a7-cb5c447b6bc2

[13] Li, X., Zhao, X., Zhang, Z., Avelin, A., Liu, S., & Li, H. (2025). Selecting cooling methods for electric motors. Applied Thermal Engineering, 274, 126554.

[14] Madukasi, A. H., Onyenanu, I. U., Oghenekaro, P. O., Nzenwa, C. C., & Madu, K. E. (2025). Optimization of the Drying Parameters for Plantain Chips using a Locally Made Tray Dryer: A Study on Drying Efficiency and Drying Rate Modeling using RSM. JournalofFoodTechnology&NutritionSciences, 206(7), 2–10. DOI: Doi. Org/10.47363/JFTNS/2025

[15] Nwigbo, O., Nwoko, C., Emerie, S., & Onyenanu, I. (2025). Optimizing Agricultural Drying Technologies: A Systematic Review of Charcoal, Gas, and Hybrid Kilns for Sustainable Food Preservation. Journal of Sustainable Engineering & Renewable Energy (JSERE), 1(1), 37–51.

[16] Offodum, C. D., Oji, A., & Onyenanu, I. U. (2025). Optimization of Inorganic Refrigerants in Cascade LNG Liquefaction Systems: A Response Surface Methodology Approach for Enhanced Energy Efficiency and Sustainability. Journal of Engineering and Applied Sciences Technology. SRC/JEAST-426. DOI: Doi. Org/10.47363/JEAST/2025 (7), 306, 2–9.

[17] Okpala, I. F., Onyenanu, I. U., Ezechukwu, V. C., & Ilochonwu, C. E. (2025). Performance Optimization of a Locally Developed Charcoal Briquette Machine Using Response Surface Methodology. Scientific Journal of Engineering, and Technology, 2(1), Article 1. https://doi.org/10.69739/sjet.v2i1.486

[18] Onyegirim, S., Onyenanu, I., Madukasi, A., & Nwigbo, O. (2025). The Role of Intake Manifold Geometry on Airflow Dynamics and Combustion Efficiency: A Computational and Experimental Review. Journal of Sustainable Engineering & Renewable Energy (JSERE), 1(1), 29–36.

[19] Onyenanu, I. U., & Nwigbo, S. C. (2021). Optimization of aluminium metal matrix composite (AMMC) for use in automobile brake disc. Int.J.Eng.Res.Technol, 10(7), 634–638.

[20] Onyenanu, I. U., Ogbogu, M. C., & Nwadiuto, C. J. (2024b). Performance optimization of an improved biomass gasifier charcoal stove using response surface method (RSM). International Journal of Engineering Research & Technology (IJERT), 13(08). DOI: 10.17577/IJERTV13IS080031

[21] Onyenanu, I. U., Ukwu, N. O., Ezechukwu, V. C., Onyenanu, I. M., & Nwadiuto, C. J. (2024a). Modelling and Optimization of Banana/Plantain Fiber Extraction Systems through Dimensional Analysis. InternationalJournalofAppliedand NaturalSciences,2(2), 40–52. https://doi.org/10.61424/ijans.v2i2.161

[22] Pereira, R. J. R., de Almeida, F. A., & Gomes, G. F. (2023). A multiobjective optimization parameters applied to additive manufacturing: DOE-based approach to 3D printing. Structures, 55, 1710–1731. https://doi.org/10.1016/j.istruc.2023.06.136

[23] Petrova, S., & Dimitrov, I. (2025). Systematic Parameter Tuning for Multi-Objective Optimization Problems Through Statistical Experimental Design. Frontiers in Emerging Artificial Intelligence and Machine Learning, 2(06), 14–26.

[24] Rachman, N. A., & Risdiyanto, A. (2015). Performance evaluation of electric motor based on review of bearing lifetime and windings temperature. International Journal of Applied Engineering Research, 10, 38070–38077.

[25] Sethupathi, P., & Senthilnathan, N. (2020). Comparative analysis of line-start permanent magnet synchronous motor and squirrel cage induction motor under customary power quality indices. Electrical Engineering, 102(3), 1339–1349. https://doi.org/10.1007/s00202-020-00955-2

[26] Shirazi, M., Khademalrasoul, A., & Safieddin Ardebili, S. M. (2020). Multi-objective optimization of soil erosion parameters using response surface method (RSM) in the Emamzadeh watershed. Acta Geophysica, 68(2), 505–517. https://doi.org/10.1007/s11600-020-00404-5

[27] Usca-Gomez, H. G., Puma-Benavides, D. S., Zambrano-Leon, V. D., Castillo-Díaz, R., Quinga-Morales, M. I., Solís-Santamaria, J. M., & Llanes-Cedeño, E. A. (2025). A Review and Case of Study of Cooling Methods: Integrating Modeling, Simulation, and Thermal Analysis for a Model Based on a Commercial Electric Permanent Magnet Synchronous Motor. World Electric Vehicle Journal, 16(8), 437. https://doi.org/10.3390/wevj16080437

[28] Wang, Q., Wu, Y., Niu, S., & Zhao, X. (2022). Advances in Thermal Management Technologies of Electrical Machines. Energies, 15(9), 3249. https://doi.org/10.3390/en15093249

[29] Wang, R., Fan, X., Li, D., Qu, R., Liu, Z., & Li, L. (2022). Comparison of heat transfer characteristics of the hollow-shaft oil cooling system for high-speed permanent magnet synchronous machines. IEEE Transactions on Industry Applications, 58(5), 6081–6092. https://doi.org/doi:%252010.1109/TIA.2022.3182312.